PHYSICAL REVIEW E **88**, 033003 (2013)

Time persistence of floating-particle clusters in free-surface turbulence

Salvatore Lovecchio,[1] Cristian Marchioli,[1,2,3] and Alfredo Soldati[2,3,*]

[1] *Dipartimento di Ingegneria Elettrica, Gestionale e Meccanica, Università degli Studi di Udine, 33100, Udine, Italy*

[2] *Centro Interdipartimentale di Fluidodinamica e Idraulica, Università degli Studi di Udine, 33100, Udine, Italy*

[3] *Dipartimento di Fluidodinamica, CISM, 33100, Udine, Italy*

(Received 23 April 2013; revised manuscript received 5 June 2013; published 5 September 2013)

We study the dispersion of light particles floating on a flat shear-free surface of an open channel in which the flow is turbulent. This configuration mimics the motion of buoyant matter (e.g., phytoplankton, pollutants, or nutrients) in water bodies when surface waves and ripples are smooth or absent. We perform direct numerical simulation of turbulence coupled with Lagrangian particle tracking, considering different values of the shear Reynolds number ($\mathrm{Re}_\tau = 171$ and 509) and of the Stokes number ($0.06 < \mathrm{St} < 1$ in viscous units). Results show that particle buoyancy induces clusters that evolve towards a long-term fractal distribution in a time much longer than the Lagrangian integral fluid time scale, indicating that such clusters overlive the surface turbulent structures which produced them. We quantify cluster dynamics, crucial when modeling dispersion in free-surface flow turbulence, via the time evolution of the cluster correlation dimension.

DOI: 10.1103/PhysRevE.88.033003 PACS number(s): 47.55.Kf, 47.27.−i

I. INTRODUCTION

Buoyant particles transported by three-dimensional incompressible turbulence are known to distribute nonuniformly within the flow [1–4]. In the particular case of light tracer particles (referred to as floaters hereinafter) in free-surface turbulence, nonuniform distribution is observed on the surface, where floaters form clusters by accumulating along patchy and string-like structures [3]. Clustering occurs even if floaters have no inertia and in the absence of floater-floater interaction, surface tension effects, or wave motions [3]. Differently from the case of inertial particles, in which clustering is driven by inertia and arises when particle trajectories deviate from flow streamlines [5], clusters are controlled by buoyancy, which forces floaters on the surface. The physical mechanism governing buoyancy-induced clustering is closely connected to the peculiar features of free-surface turbulence, which is characterized by sources (sinks) of fluid velocity where the fluid is moving upward (downward) [1]. Once at the surface, floaters follow fluid motions passively and leave quickly the upwelling regions gathering in downwelling regions: here, fluid can escape from the surface and sink whereas floaters cannot, precisely because of buoyancy [3].

In a series of recent papers [2–4] it was shown that floater clusters in free-surface turbulence form a compressible system that evolves towards a fractal distribution in several large-eddy turnover times (measured at the free surface) and at an exponential rate. The macroscopic manifestation of this behavior is the strong depletion of floaters in large areas of the surface and very high particle concentration along narrow string-like regions, which are typical of scum coagulation on the surface of the sea [4]. From a statistical viewpoint, this is reflected by a peaked probability distribution function of particle concentration with power-law tails. A proper description of such power-law distribution requires a clear understanding of the mechanism by which floaters are segregated into filamentary clusters.

In this paper we examine such a mechanism from a phenomenological point of view, and we also quantify cluster dynamics in connection with the characteristic time scale of the surface vortices. This analysis is of fundamental interest since it quantifies the temporal persistency of clusters with respect to the dominant surface flow scales, but reflects practically towards modeling of dispersion in many surface transport phenomena, such as the spreading of phytoplankton, pollutants, and nutrients in oceanic flow [4].

II. PROBLEM FORMULATION AND NUMERICAL METHODOLOGY

The physical problem considered in this study is floater dispersion at the free surface of a turbulent open channel flow. A sketch of the simulated flow configuration is shown in Fig. 1, together with the boundary conditions for the fluid (water). The flow field is calculated by integrating incompressible continuity and Navier-Stokes equations. In dimensionless form:

$$\frac{\partial u_i}{\partial x_i} = 0, \tag{1}$$

$$\frac{\partial u_i}{\partial t} = -u_j \frac{\partial u_i}{\partial x_j} + \frac{1}{Re_\tau} \frac{\partial^2 u_i}{\partial x_j \partial x_j} - \frac{\partial p}{\partial x_i} + \delta_{1,i}, \tag{2}$$

with u_i the ith component of the fluid velocity, p the fluctuating kinematic pressure, $\delta_{1,i}$ the mean pressure gradient driving the flow, and $\mathrm{Re}_\tau = h u_\tau/\nu$ the shear Reynolds number based on the channel depth h and the shear velocity $u_\tau = \sqrt{h|\,\delta_{1,i}|\,/\rho}$. Equations (1) and (2) are solved directly using a pseudospectral method that transforms field variables into wave-number space, through Fourier representations for the streamwise and spanwise directions (using k_x and k_y wave numbers, respectively) and a Chebyshev representation for the wall-normal nonhomogeneous direction (using T_n coefficients). A two-level explicit Adams-Bashfort scheme for the nonlinear terms and an implicit Crank-Nicolson method for the viscous terms are employed for time advancement. More details on the numerical method can be found elsewhere [5,6].

*Corresponding author: soldati@uniud.it; +39 (0)432 558020.

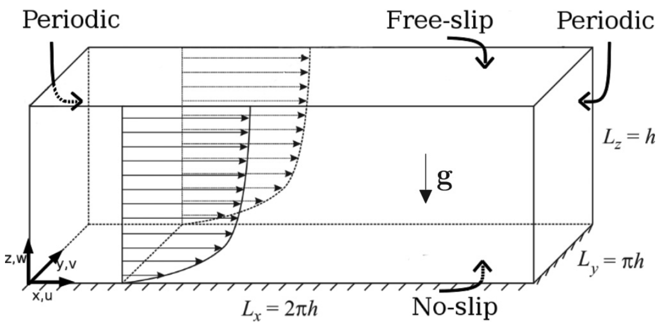

FIG. 1. Sketch of the computational domain with boundary conditions for the fluid.

The floaters motion is described by a set of ordinary differential equations for velocity $\mathbf{v}_p$ and position $\mathbf{x}_p$ at each time step. In vector form:

$$\frac{d\mathbf{x}_p}{dt} = \mathbf{v}_p, \tag{3}$$

$$\frac{d\mathbf{v}_p}{dt} = \frac{(\rho_p - \rho_f)}{\rho_p}\mathbf{g} + \frac{(\mathbf{u}_{@p} - \mathbf{v}_p)}{\tau_p}\left(1 + 0.15\,\mathrm{Re}_p^{0.687}\right), \tag{4}$$

where $\mathbf{u}_{@p}$ is the fluid velocity at the floater position, interpolated with sixth-order Lagrange polynomials, ρ_p (ρ_f) is the floater (fluid) density, and $\tau_p = \frac{\rho_p d_p^2}{18\rho_f \nu}$ is the floater relaxation time based on the diameter d_p. The Stokes drag coefficient is computed using the Schiller-Naumann nonlinear correction [7], required to ensure accurate evaluation of the drag force exerted on floaters with Reynolds number $\mathrm{Re}_p = |\mathbf{u}_{@p} - \mathbf{v}_p|\, d_p/\nu > 0.2$. To calculate individual trajectories, periodic boundary conditions are imposed on floaters moving outside the computational domain in the homogeneous directions. In the wall-normal direction, particles reaching the free-slip surface still obey the buoyancy force balance, whereas elastic rebound is enforced at the no-slip bottom wall. We remark here that the buoyancy force balance does not automatically enforce particles to stay at the free surface. Equations (3) and (4) are advanced in time using a fourth-order Runge-Kutta scheme starting from a random distribution of floaters with velocity $\mathbf{v}_p(t=0) \equiv \mathbf{u}_{@p}(t=0)$.

The results presented in this paper are relative to two values of the shear Reynolds number: $\mathrm{Re}_\tau^L = 171$ and $\mathrm{Re}_\tau^H = 509$ corresponding, respectively, to shear velocities $u_\tau^L = 0.00605$ ms^{-1} and $u_\tau^H = 0.018$ ms^{-1} for a channel depth $h \simeq 0.03m$. The size of the computational domain in wall units is $L_x^+ \times L_y^+ \times L_z^+ = 2\pi\mathrm{Re}_\tau \times \pi\mathrm{Re}_\tau \times \mathrm{Re}_\tau$, discretized with $128 \times 128 \times 129$ grid points ($k_x = i2\pi/L_x$, $k_y = j2\pi/L_y$ with $i,j = 1,\ldots,128$, and $T_n(z) = \cos[n\cos^{-1}(z/h)]$ with $n = 1,\ldots,129$ before de-aliasing) at Re_τ^L and with $256 \times 256 \times 257$ grid points ($i,j = 256$ and $n = 257$ before de-aliasing) at Re_τ^H. The grid spacing is uniform in the streamwise and spanwise directions, with $\Delta x^+ \simeq 8.46$ and $\Delta y^+ \simeq 4.23$ at Re_τ^L ($\Delta x^+ \simeq 12.54$ and $\Delta y^+ \simeq 6.27$ at Re_τ^H). The grid points along the wall-normal direction are clustered near the free surface and near the bottom wall: the minimum and maximum resolutions are $\Delta z^+_{\mathrm{min}} \simeq 0.026$ and $\Delta z^+_{\mathrm{max}} \simeq 2.1$ at Re_τ^L ($\Delta z^+_{\mathrm{min}} \simeq 0.019$ and $\Delta z^+_{\mathrm{max}} \simeq 3.12$ at Re_τ^H). For validation purposes, Fig. 2 shows the mean and root mean square (RMS) fluid velocity profiles for both Reynolds numbers: our results compare well with those reported in previous studies (see, e.g., Ref. [8], not shown). Figures 2(a) and 2(c) indicate that the free surface does not alter significantly the mean velocity profile, but also does not influence near-wall turbulence. The strong effect of the free surface on turbulence is revealed by the increase of the streamwise and spanwise components of the RMS near the surface itself [see Figs. 2(b) and 2(d)], indicating the presence of an anisotropic velocity layer [8]. For a more complete collection of flow field statistics see Ref. [9].

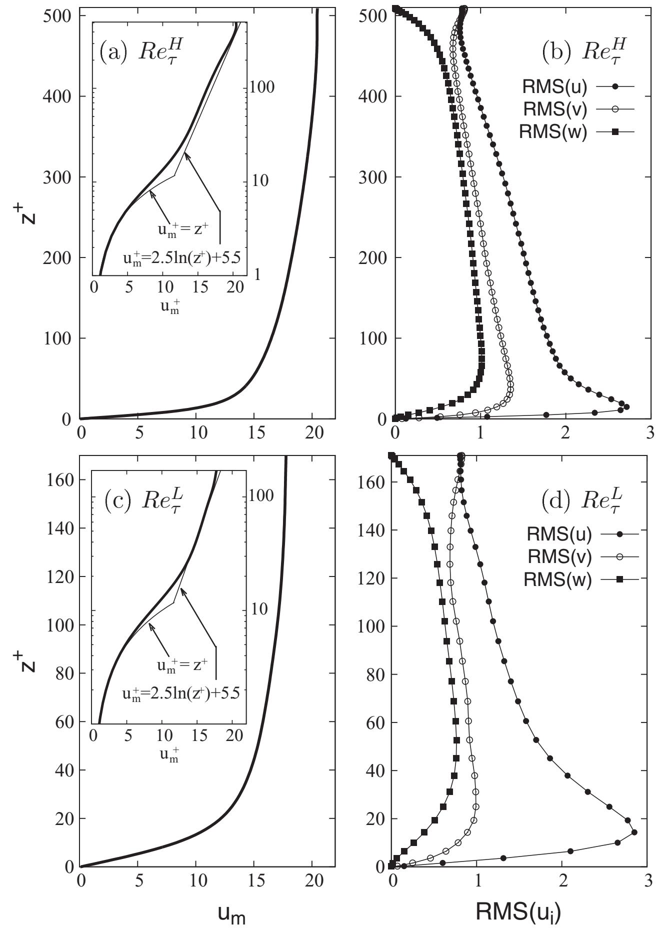

FIG. 2. Fluid velocity statistics: (a, c) mean streamwise velocity, u_m^+; and (b, d) root mean square components, RMS(u_i). Panels (a, b) refer to the Re_τ^H simulation, panels (c, d) refer to the Re_τ^L simulation. The insets in panels (a, b) compare the mean velocity profile to the wall law $u_m^+ = z^+$ and to the logarithmic law $u_m^+ = 2.5\ln(z^+) + 5.5$ in lin-log scale.

Samples of $\mathcal{N} = 2 \times 10^5$ floaters characterized by specific density $S = \rho_p/\rho_f = 0.5$ and diameter $d_p = 250\,\mu$m (a value in the size range of large phytoplankton cells [10]) were considered. The corresponding values of the nondimensional response time (Stokes number) $\mathrm{St} = \tau_p/\tau_f$ with $\tau_f = \nu/u_\tau^2$ the viscous time scale of the flow, are $\mathrm{St}^L = 0.064$ at Re_τ^L and $\mathrm{St}^H = 0.562$ at Re_τ^H. Floaters with density much less than that of the fluid were considered on purpose to confine their motion to the free surface and produce a behavior which resembles not at all that of neutrally buoyant, noninertial particles. To evaluate the integral flow scales (discussed in

Sec. III C), swarms of $\mathcal{N}$ massless fluid tracers characterized by $\mathrm{St}^L = \mathrm{St}^H = 0$ were also tracked, through the integration of Eq. (3) with $\mathbf{v}_p(t) = \mathbf{u}_{@p}(t)$.

III. RESULTS AND DISCUSSION

A. Characterization of free-surface turbulence through energy spectra

Turbulent flow structures near the free surface of an open channel have been investigated in several previous studies [6,8,11–15]. All these studies show that surface structures are generated and sustained by bursting phenomena that are continuously produced by wall-shear turbulence inside the buffer layer. Bursts emanate from the bottom of the channel and produce upwelling motions of fluid as they are convected toward the free surface. Near the surface, turbulence is restructured and nearly two-dimensionalized due to damping of vertical fluctuations [16]: upwellings appear as two-dimensional sources for the surface-parallel fluid velocity and alternate to sinks associated with downdrafts of fluid from the surface to the bulk. Through sources fluid elements at the surface are replaced with fluid from the bulk, giving rise to the well-known surface-renewal events [13]. Whirlpool-like vortices may also form in the high-shear region between closely adjacent upwellings. This phenomenology has been long recognized to produce flow with properties that differ from those typical of two-dimensional incompressible Navier-Stokes turbulence [1,17]. These properties can be quantified examining the energy spectra of the fluid velocity fluctuations on the surface [8], shown in Fig. 3 for the case of statistically steady turbulence. To emphasize the direction-related aspects of the energy spectra, results for the surface-parallel velocities are examined in isolation: Figs. 3(a) and 3(c) show the one-dimensional streamwise spectra of the streamwise velocity $E_x(k_x)$ computed at the free surface ($z^+ = 0$, circles) and at the channel center ($z^+ = 254.6$ at Re_τ^H, $z^+ = 85.5$ at Re_τ^L, squares) in the Re_τ^H and Re_τ^L simulations, respectively; Figs. 3(b) and 3(d) show the spectra of the spanwise velocity $E_y(k_x)$ in the same two regions. The solid lines represent the slope of the spectrum within the inertial regimes predicted by the Kraichnan-Leith-Batchelor (KLB) phenomenology of two-dimensional turbulence [18,19]: $k_x^{-5/3}$, representing the inverse cascade of energy to large flow scales and k_x^{-3}, representing the direct cascade of enstrophy to small flow scales. A collective analysis of the spectra shown in Fig. 3 reveals clear deviations from two dimensionality. First, no evident $-5/3$ range is observed except for few of the lowest wave numbers: this can be attributed to the intermittent nature of turbulence associated with spatial fluctuations in the rate of energy dissipation. A relatively larger range of high wave numbers can be identified over which spectra exhibit a -3 scaling: In the present flow configuration, however, this corresponds to the up-cascading of energy from large to small wave numbers, namely to the merging of smaller flow structures into larger structures. Such findings cannot be reconciled with the KLB theory for two-dimensional (2D) turbulence.

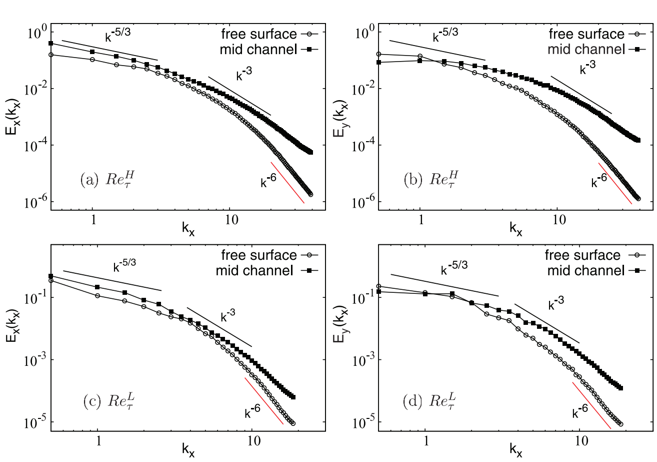

FIG. 3. (Color online) One-dimensional (streamwise) energy spectra of the streamwise [(a, c) $E_x(k_x)$] and spanwise [(b, d) $E_y(k_x)$] surface-parallel velocity fluctuations.

Examining $E_x(k_x)$, we notice that the spectrum at the free surface is always below that in the center of the channel. Also, energy in the high-wave-number portion of the spectrum decays more rapidly [8], roughly as k^{-6}: This tendency is particularly evident at Re_τ^H and indicates that only large-scale surface structures survive to the detriment of small-scale ones. Examining $E_y(k_x)$, we observe that the redistribution of energy from small to large scales in the proximity of the free surface determines a cross over between spectra at low wave numbers (for both Reynolds numbers): this finding confirms further that small scale structures play little role in determining turbulence properties in this region of the flow.

B. Characterization of particle clustering through surface divergence

Most of the analyses for geophysical flows have been conducted considering two-dimensional incompressible homogeneous isotropic turbulence [20,21]. In such flows the divergence of the velocity field is zero by construction. However, the divergence in real surface flows is defined as

$$\nabla_{2D} = \frac{\partial u}{\partial x} + \frac{\partial v}{\partial y} = -\frac{\partial w}{\partial z}, \tag{5}$$

and does not vanish. Therefore floaters, forced to stay on the surface by buoyancy, probe a compressible two-dimensional system [2], where velocity sources are regions of local flow expansion ($\nabla_{2D} > 0$) generated by subsurface upwellings and velocity sinks are regions of local compression ($\nabla_{2D} < 0$) due to downwellings [1]. In Fig. 4 we provide a qualitative characterization of floater clustering on the free surface by correlating the instantaneous particle patterns with the colormap of ∇_{2D}. Due to buoyancy, floaters reaching the free surface cannot retreat from it following flow motions: they can only leave velocity sources (the red areas in Fig. 4) and collect into velocity sinks (the blue areas in Fig. 4). Once trapped in these regions, floaters organize themselves in clusters that are stretched by the fluid forming filamentary structures. Eventually sharp patches of floater density distribution are produced, which correlate very well with the rapidly changing patches of ∇_{2D}, as clearly shown by Fig. 4. Similar behavior (the formation of clusters with fractal mass distribution) has been observed in previous studies [2,3] for the case of Lagrangian tracers in surface flow turbulence without mean shear.

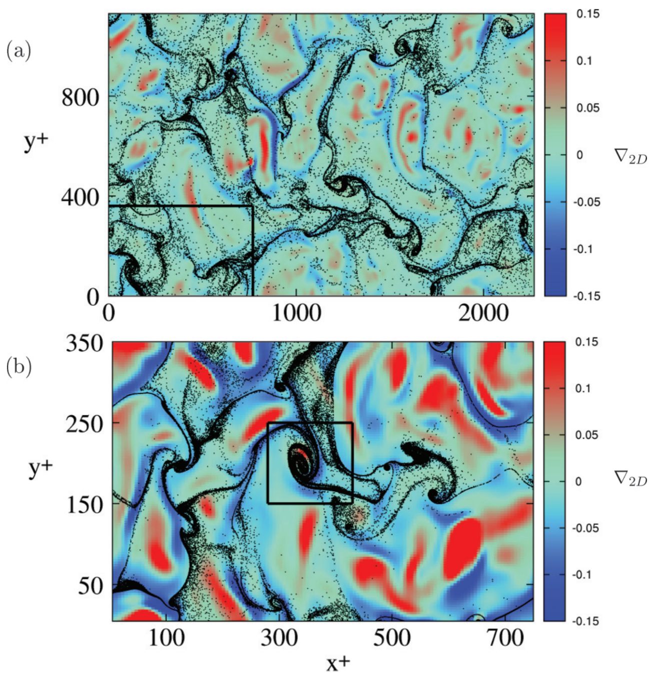

FIG. 4. (Color online) Correlation between floater clusters and surface divergence ∇_{2D}: floaters segregate in $\nabla_{2D} < 0$ regions (in blue, footprint of subsurface downwellings) avoiding $\nabla_{2D} > 0$ regions (in red, footprint of subsurface upwellings). (a) Re_τ^H, $t^+ = 180$ upon floater injection; (b) Re_τ^L, $t^+ = 121$. The rectangle in panel (a) renders the relative domain size in the Re_τ^L simulation; the rectangle in panel (b) highlights the floater cluster shown in Fig. 6.

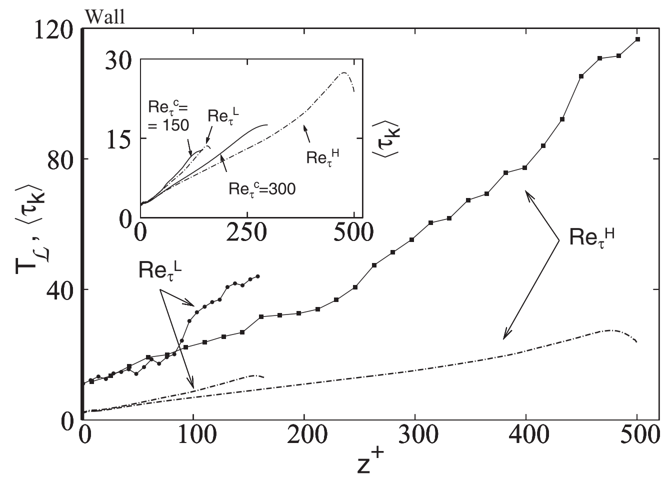

FIG. 5. Lagrangian integral fluid time scale ($T_{\mathcal{L}}$, symbols) and Kolmogorov time scale ($\langle\tau_K\rangle$, lines) in open channel flow at Re_τ^H (squares) and at Re_τ^L (circles), as function of the wall-normal coordinate z^+. The inset compares the behavior of $\langle\tau_K\rangle$ in open channel flow with that in closed channel flow (at $\mathrm{Re}_\tau^c = 150$ and 300, solid lines).

C. Time scaling of floaters clustering

Due to the close phenomenological connection between clustering and surface turbulence, the cluster length and time scales are expected to depend on local turbulence properties. In particular, one can quantify the temporal coherence of surface flow structures through their Lagrangian integral time scale (equivalently, their eddy turnover time [1]):

$$T_{\mathcal{L},ij} = \int_0^\infty R_{f,ij}[t,\mathbf{x}_f(t)]dt, \tag{6}$$

where

$$R_{f,ij}[t,\mathbf{x}_f(t)] = \frac{\langle \mathbf{u}'_{f,i}[t,\mathbf{x}_f(t)] \cdot \mathbf{u}'_{f,j}[t_0,\mathbf{x}_f(t_0)]\rangle}{\langle \mathbf{u}'_{f,i}[t_0,\mathbf{x}_f(t_0)] \cdot \mathbf{u}'_{f,j}[t_0,\mathbf{x}_f(t_0)]\rangle} \tag{7}$$

is the correlation coefficient of velocity fluctuations. Correlation coefficients were obtained upon ensemble-averaging (denoted by angle brackets) over all $\mathcal{N}$ fluid tracers released within the flow domain. Subscript f denotes the dependence of $R_{f,ij}$ on the instantaneous tracer position $\mathbf{x}_f(t)$. Velocity fluctuations were computed as $\mathbf{u}'_{f,i}[t,\mathbf{x}_{f,i}(t)] = \mathbf{u}_{f,i}[t,\mathbf{x}_{f,i}(t)] - \bar{\mathbf{u}}_{f,i}[t,\mathbf{x}_{f,i}(t)]$, with $\bar{\mathbf{u}}_{f,i}[t,\mathbf{x}_{f,i}(t)]$ the space-averaged Eulerian fluid velocity. The estimation of $T_{\mathcal{L},ij}$ is crucial to parametrize particle spreading rates and model large-scale diffusivity in bounded shear dispersion [22]. To compute $T_{\mathcal{L},ij}$ we divided the channel height into 50 uniformly spaced bins filled with tracers. For each tracer we computed the instantaneous value of the diagonal elements of $R_{f,ij}$ and their integral over time to get $T_{\mathcal{L},11}$, $T_{\mathcal{L},22}$, and $T_{\mathcal{L},33}$. Finally, these were ensemble-averaged within each bin using only tracers initially located within the bin.

In Fig. 5 we show, for both Re_τ^H and Re_τ^L, the wall-normal behavior of the Lagrangian integral time scale of the fluid (symbols), obtained as $T_{\mathcal{L}} = [\langle T_{\mathcal{L},11}\rangle + \langle T_{\mathcal{L},22}\rangle + \langle T_{f,33}\rangle]/3$. Note that $\langle T_{\mathcal{L},33}\rangle \simeq 0$ at the surface. For comparison purposes, the Kolmogorov time scale $\langle\tau_K\rangle$, is also shown (dot-dashed line). The value of $T_{\mathcal{L}}$ changes significantly with the distance from the wall: in the Re_τ^H simulation, $T_{\mathcal{L}} \simeq 120$ at the surface, a value ten times larger than that near the wall (where $T_{\mathcal{L}} \simeq 14$) indicating that the characteristic lifetime of surface structures is significantly longer than that of near-wall structures. It is also evident that $T_{\mathcal{L}}$ is everywhere larger than $\langle\tau_K\rangle$, confirming clear scale separation between large-scale surface motions and small-scale dissipative structures.

To correlate the typical lifetime of surface motions with that of floater clusters, we examine next the time-evolution of the local correlation dimension of clusters $D_2(t)$ [4]. The same observable was studied experimentally also by Larkin *et al.* [3,4] as a measure of the fractal dimension of floater distribution. Their main finding is that $\langle D_2(t)\rangle$ decays at an exponential rate from $\langle D_2(t=0)\rangle \simeq 2$ to $\langle D_2(t\to\infty)\rangle \simeq 1$, the decay time being approximately one surface eddy turnover time (defined as the typical time for the "largest" eddies to significantly distort in a turbulent flow). In this work, we computed $D_2(t)$ for several surface clusters, one of which is followed in time in Fig. 6. This particular cluster was generated by past upwelling motions, which it survived [Fig. 6(a)], and is now found sampling a region of the free-surface reached by another upwelling motion [Fig. 6(b), red area]. Floaters are swept from the velocity source and redistribute at its edges maintaining the cluster spatial connection, as shown in Fig. 6(c). As time progresses [Fig. 6(d)], the cluster reshapes generating sharp density fronts.

Upon isolating the floaters subsample Φ_j for each cluster forming on the surface, we computed at each time step the

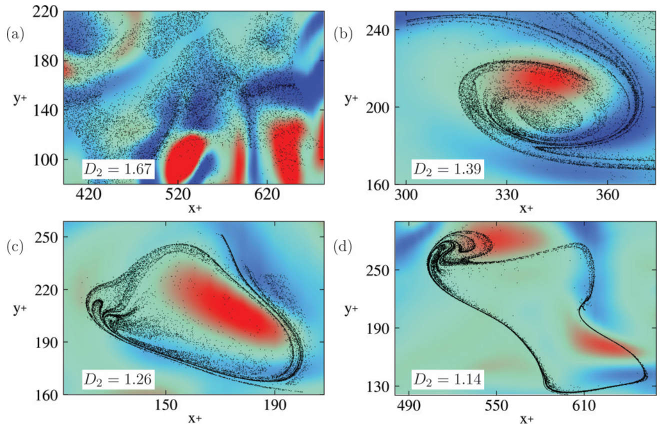

FIG. 6. (Color online) Time evolution of the floater cluster highlighted in Fig. 4(b). The cluster is examined following its Lagrangian path, with Eulerian coordinates in each snapshot changing accordingly. Upon reaching the surface within an upwelling, floaters start to collect into a neighboring downwelling (blue region) at time $t^+ \simeq 36 \simeq 0.7T_{\mathcal{L}}$. Then, they are hit by a subsequent upwelling (red region) at (a) time $t^+ \simeq 121 \simeq 2.4T_{\mathcal{L}}$, and (b) scattered around at time $t^+ \simeq 145 \simeq 2.9T_{\mathcal{L}}$. (c) Eventually, they form a highly concentrated filamentary pattern at time $t^+ \simeq 193 \simeq 3.9T_{\mathcal{L}}$. This pattern exhibits strong time persistency and overlives several surface-renewal events.

conditioned correlation dimension $D_2(\Phi_j,t)$. The instantaneous value of $D_2(\Phi_j,t)$ for the specific cluster examined in Fig. 6 is given in each figure panel and shows a decrease in time associated to the formation of filamentary clusters: $D_2(\Phi_j,t) \simeq 1.67$ at relatively short times [$t \simeq 0.7T_{\mathcal{L}}$, Fig. 6(a)]; and $D_2(\Phi_j,t) \simeq 1.14$ at much larger times [$t \simeq 3.9T_{\mathcal{L}}$, Fig. 6(d)]. These values are also included as circles in Fig. 7(b), where we show the time behavior of the ensemble-averaged correlation dimension: $\langle D_2(t)\rangle = \sum_{j=1}^{\mathcal{N}_c} D_2(\Phi_j,t)$ (red line), with $\mathcal{N}_c$ the number of clusters over which averaging was made ($\mathcal{N}_c = 10$ for the profiles shown in Fig. 7). To render the intermittency of the clustering phenomenon, and to quantify the uncertainty associated with our measurement, we also plot the standard deviation from $\langle D_2(t)\rangle$ (error bars). The black line in each panel represents the estimate of $\langle D_2(t)\rangle$ obtained assuming an exponential decay rate [3,4]. In the present flow configuration, the decay time is given as proportional to the value of $T_{\mathcal{L}}$ at the free surface. The best fit to the data is given by a relation of the type $\langle D_2(t) - D_2(\infty)\rangle \propto \exp(-t/\alpha T_{\mathcal{L}})$ with $\alpha \simeq 5$ for both Re_τ^H and Re_τ^L. This result proves the long-time persistency of surface clusters that evolve in a time significantly larger than $T_{\mathcal{L}}$ to a steady state where the measured $\langle D_2(t)\rangle$ approaches a value approximately equal to 1, in agreement with the formation of the filament-like structures observed in Fig. 6. The present findings confirm qualitatively those of Larkin *et al.* [3,4], but show a slower decay time (larger than $T_{\mathcal{L}}$ and, in turn, larger than one eddy turnover time). This may be due to the different three-dimensional (3D) flow instance considered below the 2D free surface. We also remark that $\langle D_2(t)\rangle$ has an asymptotic behavior because of the noninteracting point-particle assumptions adopted. More realistic physical modeling for particles interacting with surface forces could lead to different long-time behavior.

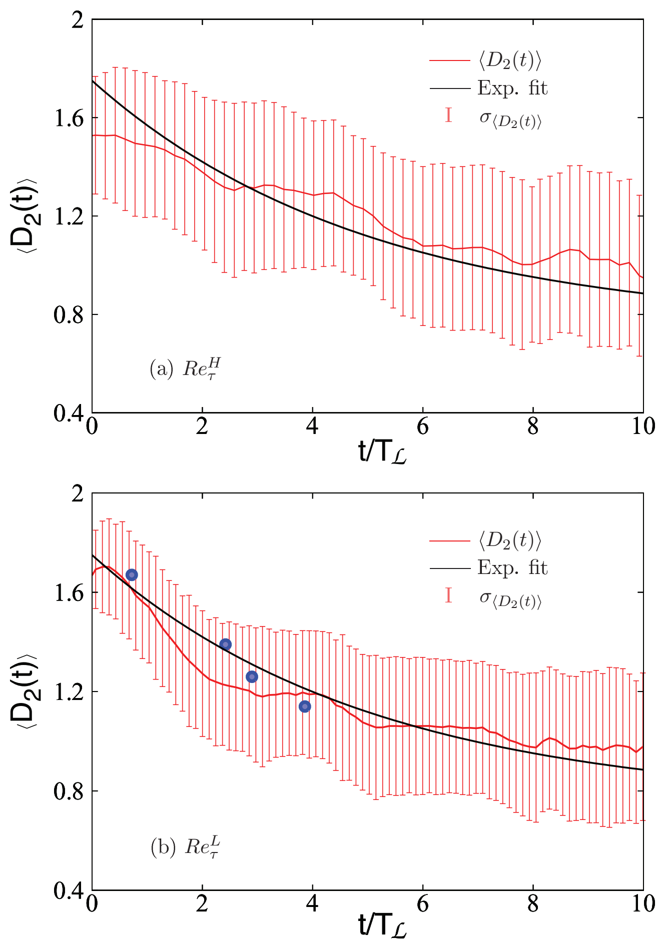

FIG. 7. (Color online) Time evolution of the cluster correlation dimension $\langle D_2(t)\rangle$ at the free surface. Circles in panel (b) represent the instantaneous values of D_2 for the floater cluster shown in Fig. 6.

IV. CONCLUSION

This study highlights the intermittent character of particle spatial distribution in free-surface turbulence. Intermittency is due to the buoyancy-driven clustering effects connected to the formation of sources and sinks of fluid velocity generated by subsurface upwelling and downwelling motions. At small time scales, cluster formation is driven by the divergence of the flow field at the surface: Clusters evolve in time producing fractal-like patterns that can be characterized by their correlation dimension. Our results indicate that these patterns slowly relax towards a long-term distribution with exponential decay rate, requiring several Lagrangian integral fluid time scales. According to the authors of Refs. [13,14], the surface-renewal time scale, which is usually employed to quantify interface scalar fluxes, is much smaller than the Lagrangian time scale and is thus inappropriate to quantify floater distribution dynamics.

Surface compressibility may play an important role in determining the motion of passive tracers like pollutants and nutrients, but also the spreading rate of active ocean surfactants, such as phytoplankton [2]. Our findings provide useful indications to parametrize the relevant time scales characterizing the dispersion of such species and, therefore, can assist in developing models to predict cluster formation and evolution over several surface renewal cycles [22]. Future developments could incorporate the strict physical connection between simulated cluster dynamics and real systems at much longer times. In particular, the effects due to particle finite size (nonoverlapping) and surface tension (that attracts particles at the surface) [23] should be considered.

[1] B. Eckhardt and J. Schumacher, Phys. Rev. E **64**, 016314 (2001).
[2] J. R. Cressman, J. Davoudi, W. I. Goldburg, and J. Schumacher, New J. Phys. **6**, 53 (2004).
[3] J. Larkin, M. M. Bandi, A. Pumir, and W. I. Goldburg, Phys. Rev. E **80**, 066301 (2009).
[4] J. Larkin, W. I. Goldburg, and M. M. Bandi, Physica D **239**, 1264 (2010).
[5] A. Soldati and C. Marchioli, Int. J. Multiphase Flow **35**, 827 (2009).
[6] Y. Pan and S. Banerjee, Phys. Fluids **7**, 1649 (1995).
[7] V. L. Schiller and A. Naumann, Z. Ver. Deut. Ing. **77**, 318 (1933).
[8] R. Nagaosa and R. A. Handler, Phys. Fluids **15**, 375 (2003).
[9] http://cfd.mace.manchester.ac.uk/ercoftac/.
[10] J. Ruiz, D. Macias, and F. Peters, Proc. Natl. Acad. Sci. U.S.A. **101**, 17720 (2004).
[11] S. Komori, H. Ueda, F. Ogino, and T. Mizushina, Int. J. Heat Mass Transfer **25**, 513 (1982).
[12] M. Rashidi and S. Banerjee, Phys. Fluids **31**, 2491 (1988).
[13] S. Komori, Y. Murakami, and H. Ueda, J. Fluid Mech. **203**, 103 (1989).
[14] A. Kermani, H. R. Khakpour, L. Shen, and T. Igusa, J. Fluid Mech. **678**, 379 (2011).
[15] R. Nagaosa and R. A. Handler, AIChE J. **58**, 3867 (2012).
[16] T. Sarpkaya, Annu. Rev. Fluid. Mech. **28**, 83 (1996).
[17] S. Kumar, R. Gupta, and S. Banerjee, Phys. Fluids **10**, 437 (1998).
[18] R. H. Kraichnan, Phys. Fluids **10**, 1417 (1967).
[19] G. K. Batchelor, Phys. Fluids **12**, 233 (1969).
[20] D. G. Dritschell and B. Legras, Phys. Today **46**, 44 (1993).
[21] P. Tabeling, Phys. Reports **362**, 1 (2002).
[22] M. S. Spydell and F. Feddersen, J. Fluid Mech. **691**, 69 (2012).
[23] P. Singh, D. D. Joseph, and N. Aubry, Soft Matter **6**, 4310 (2010).